06-8602/6

N00014-85-C-0206

(2)

FRACTURE MICROMECHANICS OF INTERMETALLIC AND CERAMIC MATRIX CONTINUOUS FIBER COMPOSITES

Interim Technical Report

Prepared for

Office of Naval Research
800 North Quincy St.
Arlington, VA 22217

By D. L. Davidson

Southwest Research Institute
P.O. Box 28510
San Antonio, TX 78284

May 1991

SOUTHWEST RESEARCH INSTITUTE
SAN ANTONIO
DETROIT
HOUSTON
WASHINGTON, DC

REPORT DOCUMENTATION PAGE

Form Approved OMB No. 0704-0188 Exp.Date: Jun 30, 1986

1a. REPORT SECURITY CLASSIFICATION UNCLASSIFIED	1b. RESTRICTIVE MARKINGS
2a. SECURITY CLASSIFICATION AUTHORITY	3. DISTRIBUTION/AVAILABILITY OF REPORT Unlimited
2b. DECLASSIFICATION/DOWNGRADING SCHEDULE	
4. PERFORMING ORGANIZATION REPORT NUMBER(S) 06-8602/6	5. MONITORING ORGANIZATION REPORT NUMBER(S) 4313283-02
6a. NAME OF PERFORMING ORGANIZATION Southwest Research Institute 6b. OFFICE SYMBOL *(If applicable)*	7a. NAME OF MONITORING ORGANIZATION Dr. Steven G. Fishman - Code 431N Office of Naval Research
6c. ADDRESS *(City, State, and ZIP)* 6220 Culebra Road P. O. Drawer 28510 San Antonio, TX 78228-0510	7b. ADDRESS *(City, State, and ZIP Code)* 800 Quincy St. Arlington, VA 22217-5000
8a. NAME OF FUNDING/SPONSORING ORGANIZATION Office of Naval Research 8b. OFFICE SYMBOL *(If applicable)*	9. PROCUREMENT INSTRUMENT IDENTIFICATION NUMBER N00014-85-C-0206
8c. ADDRESS *(City, State, and ZIP)* 800 Quincy St. Arlington, VA 22217-5000	10. SOURCE OF FUNDING NUMBERS PROGRAM ELEMENT NO. / PROJECT NO. / TASK NO. / WORK UNIT ACCESSION NO.

11. TITLE *(Include Security Classification)*
Fracture Micromechanisms of Intermetallic and Ceramic Continuous Fiber Composites

12. PERSONAL AUTHOR(S)
D. L. Davidson

13a. TYPE OF REPORT	13.b TIME COVERED	14. DATE OF REPORT *(Year, Month, Day)*	15. PAGE COUNT
Technical	FROM 4/29/90 TO 4/29/91	May 1991	43

16. SUPPLEMENTARY NOTATION

17. COSATI CODES			18. SUBJECT TERMS *(Continue on reverse if necessary and identify by block number)*
FIELD	GROUP	SUB-GROUP	Key Words: Metal matrix composites, SCS-6, SiC fiber reinforced, fracture mechanics, fatigue crack growth, crack growth micromechanisms

19. ABSTRACT *(Continue on reverse if necessary and identify by block number)*

Fatigue cracks were grown perpendicular to SCS-6 fibers in center-notched Ti-6Al-4V matrix composites made by the foil-fiber method. Displacements were measured in fibers through small access ports electropolished through the matrix. Fiber stresses were calculated from displacements. Crack growth rates and crack opening displacements were also measured. Analyses of these parameters allowed a determination of interfacial shear strength. Fracture mechanics was used to correlate the micromechanical parameters measured.

20. DISTRIBUTION/AVAILABILITY OF ABSTRACT	21. ABSTRACT SECURITY CLASSIFICATION
X UNCLASSIFIED/UNLIMITED ☐ SAME AS RPT. ☐ DTIC USERS	UNCLASSIFIED

22a. NAME OF RESPONSIBLE INDIVIDUAL	22b. TELEPHONE *(Include Area Code)*	22c. OFFICE SYMBOL
D. L. Davidson	512/522-2314	

DD FORM 1473 84 MAR 83 APR edition may be used until exhausted. All other editions are obsolete.

The micromechanics of fatigue crack growth in Ti-6Al-4V reinforced with SiC continuous fiber SCS-6 at 25°C

D.L. Davidson
Southwest Research Institute
San Antonio, TX 78228-0510

ABSTRACT

Micromechanics parameters for fatigue cracks growing perpendicular to fibers were measured for the center notched specimen geometry. Fiber displacements, measured through small port holes in the matrix made by electropolishing, were used to determine fiber stresses, which ranged from 1.1 to 4 GPa. Crack opening displacements at maximum load and residual crack opening displacements (at minimum load) were measured. Matrix was removed along the crack flanks after completion of the tests to reveal the extent and nature of the fiber damage. Analyses were made of these parameters, and it was found possible to link the extent of fiber debonding to residual COD and the shear stress for debonding, estimated at 245 MPa, to COD. Measured experimental parameters were used to compute crack growth rates using a well known fracture mechanics model for fiber bridging tailored to these experiments.

INTRODUCTION

The potential for microstructural manipulation to yield further increases in fatigue crack growth resistance for the metals and alloys currently being used in gas turbine construction is small. Studies of fatigue crack growth through aluminum, titanium and superalloys have shown that there are many similarities in the mechanisms of crack growth and the crack tip micromechanics for these materials. Conversely, materials reinforced with continuous strong fibers offer the promise of drastic increases in fatigue crack growth resistance because additional mechanisms are brought to play by composite construction.

For currently used aerospace materials, fracture mechanics has been used extensively for describing fatigue crack growth in damage tolerant design procedures. However, the appropriate uses of fracture mechanics to describe crack growth through continuous fiber metal matrix composites are still being developed. Fracture mechanics has been extended to describe fatigue crack

growth through composites with relatively strong interfaces [1,2]. But such materials offer only limited advantage over conventional materials because crack growth remains self similar [2,3].

The limited potential for composites with strong interfaces was recognized, so newer classes of materials are being engineered with somewhat weaker interfaces, which results in fiber bridging as the mechanism dominant in providing fatigue crack growth resistance. The composite discussed in this paper has a matrix of conventional titanium alloy reinforced with silicon carbide fibers. Use of fracture mechanics to describe fatigue crack growth in this materials has just begun. There is an extensive literature in laboratory and contractor reports on mechanical properties of titanium matrix composites, but much less information has been published. Only data in the published literature is referenced in this paper. Gerold [4] has reviewed most of the research on continuous fiber metal matrix composites through 1987, and should be referred to for earlier work.

Theoretical analyses of crack growth with fiber bridging have considered mainly the fracture of brittle matrix (ceramic) composites under unidirectional loading; thus, these analyses may not be directly applicable to fatigue crack growth in composites with ductile matrices. Potentially, the theoretical analyses by Budianski and Hutchinson [5], Marshall, Cox and Evans [6], McCartney [7], and McMeeking and Evans [8] are applicable to the experimental work described in this paper.

DESCRIPTION OF EXPERIMENTAL AND MEASUREMENT TECHNIQUES

Materials and Specimens

Specimens of composite made by the foil-fiber technique were used for fatigue crack growth experiments. The material was obtained from GE Aircraft Engines Company, who procured it from Textron Specialty Materials Co., manufacturer of the fibers, who also consolidated the composite. A general description of this material has been given in previous publications [9,10], so it is necessary only to specify properties for the specific panel of composite used in this research.

The composite used had 42 vol.% SCS-6 fibers arranged in 4 layers aligned in

one direction and embedded in a matrix of Ti-6Al-4V, an $\alpha + \beta$ alloy heat treated and deformed in the manufacturing process to give approximately equiaxed α grains separated by discontinuous β, generally described as a recrystallized annealed (RA) microstructure. The resulting composite is shown in **Fig. 1**. Some of the elastic properties of the materials relevant to this research are given in **Table 1**. The temperature of consolidation was between 900 and 1100°C. The resulting composite panel was not completely flat in the fiber direction. Reasons for this bow are not known because other details of the consolidation process are unavailable.

The specimens tested, which were configured to fit a specially designed cyclic loading stage for a scanning electron microscope [11], were 54 mm long, with a gauge section 24 mm wide and 0.94 mm thick. Tabs of the matrix alloy were spot welded to each end of the specimen for pin loading. Four specimens of this configuration, all cut from the same composite plate, were tested and gave similar results. Electro-discharge machining was used to cut notches approximately 0.5 mm wide in the center of these specimens perpendicular to the fiber direction. Lengths of the notches varied between 8 and 10 mm. One single edge notched specimen of the same general configuration was also tested.

Cyclic loading of the center notched specimens easily initiated cracks from each end of the notch that grew perpendicular to the loading axis on one side of the specimen, but cracks did not so readily initiate on the other side of the specimen. The bow in the specimens was thought to be the reason for this behavior. The cracks that easily initiated were on the concave side of the specimen. Eventually, cracks initiated and grew on the other side also, but crack length was never equal on both sides of the specimens. For the edge notched configuration, a crack initiated perpendicular to the fibers on one side, but parallel to the fibers on the other, and growth continued in these directions until the experiment was terminated.

Three of the center notched specimens were prepared by electropolishing each side lightly to remove scratches, followed by an etch to reveal the microstructure and create surface texture. Lacquer was used to prevent electrochemical attack in all but a small portion of the specimen gauge section.

The forth specimen was initially prepared in the same way as the others, but additional steps were taken to expose the first layer of fibers on one side of

the specimen. The objective of this effort was to remove a minimum of material, thereby disturbing the residual stresses in the composite as little as possible. Therefore, after cracks were initiated and grown approximately 0.8 mm from the starting notch, ion etching was used to remove material in a 0.5 mm wide band extending out from each end of the notch on the cracked side. The resulting trenches in the matrix were approximately 0.1 mm deep. The surface topography resulting from ion etching revealed the location of the still buried fibers because material was removed to a slightly greater depth between fibers. This surface undulation was revealed by glancing light. The entire specimen was then masked using lacquer, except for small regions directly over the fiber locations, and these regions were electropolished until the fiber was uncovered. Since each fiber was not at a uniform distance below the surface, this process required considerable patience and numerous masking and stripping operations. The resulting "access ports" to the fibers were elongated in the fiber axis direction, with this dimension varying from 50 to 150 μm. In the fiber circumferential direction, the port size was 20 to 60 μm, or 5 to 15 % of the fiber circumference.

After the fiber ports, ion etching was used again to create surface texture with minimal removal of additional material. However, this etching also removed some of the outer layer of the SCS-6 fibers where they were exposed in the ports. Some of the results of this preparation effort are shown in **Figs. 2 and 3**. An overall view of crack 1 in Specimen 4 is shown in **Fig. 2(a)**, with a higher magnification view of several of the ports to fibers shown in **Fig. 2(b)**, along with the end of the crack. More detailed views of two of the fiber access ports are shown in **Fig. 3**. The columnar structure seen on the fiber surface results from removal of most of the outer carbon rich coating of the fiber by ion etching.

Experimental procedure

Cracks were initiated and grown at least 2 notch widths by cyclic loading, during which no crack growth rate data were taken. Thence, increments of cyclic loading, ΔN, ranging from 5,000 to 50,000 cycles, were applied, and increments of crack extension, Δa, were measured using a traveling microscope. From these data, crack growth rates, $\Delta a/\Delta N$, were calculated. If a ΔN resulted in no Δa, no crack growth rate was recorded. Applied stresses were held constant during one of the experiments, but increased with increasing crack

length during the others. Applied stresses were increased because initial stresses were fairly low for these specimens and had to be intensified to obtain continue crack growth. The schedule of stresses, crack lengths, and other information is given in **Table 2.** In each case, crack arrest had occurred when the applied stress was increased.

Periodically during these experiments, the specimens were transferred to a cyclic loading stage that fit within the specimen chamber of the scanning electron microscope (SEM). Thus, photographs of the crack tip and the exposed portion of the fiber and surrounding matrix, such as shown in **Fig. 3**, were made at minimum and maximum cyclic load.

Upon termination of the crack growth experiments and accompanying measurements, matrix was removed from several of the specimens by electropolishing along a band approximately 2 mm either side of the cracks, thereby exposing the first layer of fibers so that damage to these fibers could be assessed.

Measurement Methods

The displacements in fibers and matrix caused by cyclic loading were extensively measured using the stereoimaging technique [12] through the DISMAP [13] automated system. Photographs at minimum and maximum loads of areas such as shown in **Fig. 3** were analyzed. From the resulting displacement measurements, crack opening displacement (COD) was directly determined, and from the displacements in fibers and matrix, strains were computed [12]. Also COD and strains were measured in the matrix surrounding the tips of the cracks. Crack opening load was measured directly at the crack tip by making photographs as load was being applied.

RESULTS

Crack Growth Rates

The data shown in **Figs. 4, 5, and 6** indicate that crack growth rate is mostly in the range 10^{-7} to 10^{-10} m/cy and was a function of both stress, which ranged between 118 and 175 MPa, and crack length. Crack growth rates that dropped below detectible levels in 50,000 cycles ($\approx 5 \times 10^{-11}$ m/cy) were mostly

included in the data for specimens 1 and 2. For several specimens, applied stress levels were increased during the experiments because the cracks arrest. Crack arrest may be seen in Fig. 6(a), together with the effect of increasing stress, but not nearly so well in Fig. 6(b). Applied stresses and crack lengths are given in Table 1.

These results may be compared with work from GE [10] on the same composite which showed that crack growth rate is very sensitive to material processing parameters. For a stress of 490 MPa, fatigue cracks grew 1 to $4x10^{-7}$ m/cy in a specimen from one plate and 4 to $9x10^{-7}$ m/cy in a specimen from another plate. Cracks grown from a central hole by Bain and Gambone [15] at cyclic stresses of 245 to 297 MPa exhibited crack growth rates that varied between 10^{-11} and 10^{-9} m/cy with increasing crack length, and without crack arrest.

Fiber Damage

Removal of matrix by electropolishing revealed damage to the fiber that had been caused by growth of the crack. An optical photograph showing fiber damage in specimen 1 is shown in **Fig. 7**. The sketch shows the extent of the fiber damage determined at higher magnification. The damage to the fibers is mainly to the coating, as shown by the secondary electron SEM photograph of **Fig. 8**. Cracks in the outer coating of the fibers were evidently caused when cyclic loading caused debonding between carbon-rich coating and the SiC part of the fiber.

These photographs indicate that the outer part of the coating often stays attached to the matrix and debonding, which prevents the fibers from breaking as the crack passes, is between the coating and the SiC part of the fiber or in between coating layers. Note that close to the crack line, some coating is still attached to the fibers and is uncracked, but a close examination indicates that the outer part of the coating is gone, and it is the inner part of the coating that still adheres to the fiber. No fiber coating damage was found ahead of the crack tip for specimen 1, or for the fiber just behind the tip. However, some damage was evident in specimen 4 just at the crack tip. This increase in fiber damage is caused by the higher stress at which the crack was grown in specimen 4.

The region of fiber damage has been interpreted as being that part of the

fiber over which slippage occurs relative to the matrix. Slippage lowers the strain on the fibers and allows the fatigue crack to pass without breaking fibers. The extent of fiber slippage has been measured for specimens 1 and 4, and is compared in **Fig. 9**. Slip distance is a function of the level of applied stress, crack length, and the stress needed to debond the fiber from the matrix.

Residual Crack Opening Displacement

Residual stresses are present in the as-consolidated composite due to differences in coefficient of thermal expansion (CTE) between fiber and matrix. These residual stresses have been determined by analysis [9] and some effort has been made to measure them for other titanium alloy matrices [16]. At ambient temperature, fibers are in axial and radial compression due to CTE mismatch. Axial stress for the fiber/matrix combination used here is approximately -500 MPa in the fiber, 360 MPa in the matrix, and the radial stress compressing the fiber is approximately 300 MPa [9]. Matrix residual stresses determined by x-ray analysis are approximately those calculated, but fiber stresses were higher [16]. When the passage of a fatigue crack breaks the matrix and causes sliding between the fiber and matrix, the axial residual stresses are relieved, which allows the fiber to elongate and the matrix to contract. This causes a residual crack opening displacement (CODr) that is proportional to the residual stress and the slip distance. For specimen 4, CODr values were measured as a function of crack length and stress, and the results are shown in **Fig. 10**. **Table 3** gives measured values of CODr and slip length.

The analysis used to relate slip length to CODr is given in **Appendix A**. This analysis was used with the data in Fig. 10 to calculate slip distance, and the computed values are compared to those measured in **Fig. 11**. The calculation underestimates some slip distances and overestimates others because CODr at any specific fiber is constrained by the surrounding matrix. The ratio of measured to computed slip distance averaged for the 13 values shown in the figure = 0.987, leading to the conclusion that the slip distance can be derived from CODr.

Crack opening displacements

Displacements due to loading were measured in the crack wake either between each fiber (specimen 3) or at each fiber (specimen 4) using

stereoimaging. Crack opening displacement is easily determined from these displacements, and the results are shown in **Figs. 12 and 13.** COD is shown as a function of the square root of distance behind the tip because this functional form fits the data better than a linear relation; also, the same function fits COD for fatigue cracks in unreinforced matrix. The lines shown correlating Mode I COD have the form

$$COD\ I = C_o\sqrt{d} \qquad (1)$$

where d = distance from the crack tip and C_o is the slope of the line and also may be defined as the crack tip opening displacement (CTOD). By this definition, CTOD is the opening 1 μm behind the crack tip. Measured values of C_o are summarized in **Table 4.** The form of eq. (1) is that for an elastic crack; thus, it might be possible to use this information in two ways: (1) From the relationship for an elastic crack, estimate a stress intensity factor, ΔK_{elas} , and (2) compare with previous measurements of COD for fatigue cracks in unreinforced matrix material to estimate the effective stress intensity factor, ΔK_{eff} . Calculation of K from the opening displacement for an elastic crack gives $0.0025 < \Delta K_{elas} < 0.014$ MPa$\sqrt{m}$, which is clearly below any possible values that could have been driving these cracks; therefore, elastic analysis is clearly unsuitable, just as was found for unreinforced matrix.

Previously measured crack opening data for Ti-6Al-4V (RA) [17] was reanalyzed and yielded the following correlation between C_o and ΔK_{eff} :

$$C_o = -0.512 + 0.137\ \Delta K_{eff} \qquad (2)$$

Using this correlation gives for specimen 4 at 190 and 561 kcy, $\Delta K_{eff} \approx 4.0$ MPa$\sqrt{m}$, and for 1016 kcy, $\Delta K_{eff} \approx 5$ MPa$\sqrt{m}$. The relationship between fatigue crack growth rate (m/cy) and ΔK_{eff} (MPa$\sqrt{m}$) for Ti-6Al-4V (RA) is [17]

$$da/dN = 4.0\times10^{-11}\ \Delta K_{eff}^{3.0} \qquad (3)$$

Using this relationship with the ΔK_{eff} values derived gives crack growth rates of $2\text{-}5\times10^{-9}$ m/cy, which is within the band of crack growth rates measured, as shown in **Fig. 6.**

The COD values for specimen 4 measured just prior to the end of the experiment at 1016 kcy are compared in **Table 3** to slip lengths measured after matrix removal. The ratio of COD to slip length given in the last column indicates that it is approximately constant at 8.5×10^{-3}. Thus, slip length increases approximately in proportion to COD. The simplest interpretation of this is that strain in the fiber remains approximately constant, indicating that fiber stresses are approximately constant within the bridging zone. The analysis in **Appendix B** shows how this value is related to the interfacial shear stress, τ, required to cause sliding between fiber and matrix, assuming fiber sliding over the entire debond length causes damage to the fiber coating. Using this analysis gives an average estimated value of $\tau = 245$ MPa. This compares with a value of 156 MPa, as determined by Yang, et al. [18], and 266 and 275 MPa as given in Sensmeier and Wright [10], all determined by push-out tests on SCS-6 fibers with Ti-6Al-4V matrix. Le Petitcorps, et al. [19], derived a value of 180 MPa by a fragmentation test.

Fiber stresses and Interface Integrity

In specimen 4, displacements in fibers were measured from photographs taken at the extremes of loading through the electropolished ports in the matrix. In specimen 3, fiber strains were measured, but with most of the matrix in the vicinity of the crack removed, as shown in **Fig. 7**. Strains were computed from the displacements and stresses were calculated from strain and fiber modulus. The fiber stresses, σ_f, thus determined are listed in **Table 4**.

Through the fiber access ports in specimen 4, it was possible also to determine when fibers debonded from the matrix. A summary of interface integrity is given in **Table 4**. At 118 MPa (190 kcy), fibers were still bonded to the matrix, both ahead and behind the crack tip. When stress was raised to 145 MPa, fibers began to debond behind the crack tip, but the interface remained unbroken near and just ahead of the crack tip. After 561 kcy, stress was raised to 175 MPa and debonding of fibers began to occur ahead of the crack tip.

The stress experienced by a fiber is a complex function of the load level, crack length, number of bridging fibers, and the way the load partitions between uncracked and cracked regions of the composite. For comparison with measured values, a method for estimating fiber stresses was derived, and is given in

Appendix C. This estimate assumes that the uncracked part of the composite remains at gross section stress and that all the remaining load is supported equally by each unbroken bridging fiber. The fiber stresses predicted using the model for a given applied stress and crack length are dependent on the number of bridging fibers, which was not firmly established experimentally. The computed average fiber stresses given in **Table 4** in italics are based on the observed number of broken fibers.

Another estimate of the interfacial shear stress, τ, may be derived from the axial stress in the fiber at the crack plane and the COD using eq. (A11) of McCartney's analysis [7]:

$$\tau = [\sigma_f^2/COD][D(1-\upsilon^2)/4][V_m E_m/E_c E_f] \qquad (4)$$

Using the constants for this composite, Table 1, gives $\tau = 1.7 \times 10^{-5}\ \sigma_f^2/COD$, with COD in μm and stress in MPa. The values of τ calculated by this method are listed in the last column of **Table 4**. The average interface strength computed by this method is 150 MPa.

FRACTOGRAPHY

The fracture surface of one specimen was examined by optical and scanning electron microscopy. The fractures were generally along one macroscopic plane, and the most notable features were fibers protruding from the surface and holes left in the surface due to fiber fracture away from the general fracture plane. This extent of fiber pull-out was measured and found to average 0.13 mm (140 fibers, variance from 0.01 to 0.51 mm) irrespective of position along the fracture surface. About half the fibers protruded from the surface examined. A few striations were found on the matrix fracture surface.

ANALYSIS

Of the plethora of theoretical analyses made for the cracking of continuous fiber composites under conditions where fiber bridging controls the rate of growth [5-8], most of these analyses have been aimed at brittle matrix composites (ceramics), but they have also been applied to metal matrix composites [10]. The analyses, and the models that result from them, are complex and valid for only certain conditions, such as steady state crack growth.

Comparison of the predictions of these models with experiment has been rendered particularly difficult due to the mathematical forms in which the models are presented.

In this section, several relatively simple analytical methods will be used to derive information from the data given in the preceding sections. The validity of some of the published models will then be examined by comparison to experiment.

All the theoretically derived models begin with the assumption that the effect of bridging fibers on crack tip stress intensity can be computed by treating the loads carried by fibers as a pressure applied along the crack wake that opposes the applied stress. The pressure concept averages the loads on individual fibers and is thought to be valid only when the crack length is greater than the fiber spacing. None of the models was derived for the conditions used in our experiments, in that a notch is not considered to exist or fibers are assumed to break at the same rate as the crack advances. Cyclic loading has been addressed only by McMeeking and Evans [8].

The equation derived by Sneddon and Lowengrub in 1969 to give the crack tip stress intensity factor for a crack subjected to a pressure p(x) along its flanks is (as corrected by McCartney [7] to give standard K formulation):

$$K_{tip} = \{\sqrt{(4a/\pi)}\}\int\{(\sigma_a - p(x)) / \sqrt{(a^2 - x^2)}\}\, dx \qquad (5)$$

where a is the crack length and x is a coordinate in the crack direction with origin at the center line of the specimen. This equation is usually difficult to integrate because p(x) is unknown. So another approach to this problem might be to use the fracture mechanics solution for the stress intensity factor due to application of a discrete load applied at a given distance from the crack tip. The solution for this problem, available in Tada, et al. [20], is

$$K_{fiber} = \sqrt{(2/\pi)}\sum_i (P_i/\sqrt{b_i}) \qquad (6)$$

where b_i is the distance of the i^{th} bridging fiber from the crack tip and P_i is the load (per unit length) acting at b_i. Summation over the bridging fibers gives the

stress intensity factor opposing the applied stress intensity factor K_a, with the difference being the effective stress intensity factor at the crack tip

$$K_{tip} = K_a - K_{fiber} \tag{7}$$

The key to use of these analyses is knowing the pressure distribution along the bridged part of the crack, or load on individual fibers for the discrete case. In the bridging region, loading on the fibers determines the pressure distribution along that part of the crack wake, and the level of pressure depends on the crack length, fracture strength of the fibers, and the stress required to shear the fiber relative to the matrix.

The strengths of SCS-6 fibers, although measured by several investigators and the manufacturer [21, 22], are still not well characterized because only relatively large gage lengths (≈ 2 cm) have been tested. Relevant fiber gage lengths for the present experiments are closer to 0.2 mm, as surmised from the measured lengths of fiber slippage. Fiber strengths are somewhat sensitive to the specific details of the processing used for making specific lots of fibers. The shear strength of the interface is sensitive to the surface finish on the fibers, the processing parameters used in composite consolidation, and to the strength and thermal expansion characteristics of the matrix. Whether or not there is chemical bonding between matrix and fiber, the compressive radial stress in the fibers due to the matrix causes the shear stress between fiber and matrix to be large.

The experimental results indicate that stress in the fibers is approximately constant, which implies that the pressure on the crack flank, at least to a first approximation, would be constant. The evidence for this comes from the ratio between slip length along the fibers and the COD, as presented in **Table 3**. Further evidence for this comes from the dependence of COD on distance from the crack tip, eq. (1), which is the same as for unbridged cracks, only smaller in magnitude.

If pressure distribution due to fiber bridging is considered constant in the bridging zone, and zero in the notch and zone of broken fibers, then the results of the analyses made to date are not applicable, but eq. (5) is much easier to integrate, as shown in **Appendix D**, or eq. (6) may be used.

Evaluation of the integrated form of eq. (5), as given in **Appendix D**, is given in **Table** 6. Pressure was estimated by partitioning the load between cracked and uncracked areas as discussed in **Appendix C**, and fiber stress was computed from the pressure estimate depending on the length of the bridging zone. The bridging zone was known experimentally to be complete (no broken fibers) until after 561 kcy, but the last increase in stress broke fibers; the number broken has been used in making the estimates of bridging zone used in the model. Most of the computed crack growth rates are larger than the measured values by a factor of 10 to 100. This inaccuracy comes from lack of a better estimating method for pressure, as shown by the results at 871 kcy. The values designated by an asterisk were computed based on the pressures shown. This exercise indicates that a 7 to 9 % increase in pressure changes crack growth rate by a factor of 2 to 3.

Fiber stresses predicted by the model are remarkably close to those measured. The model does not account for the interface debonding observed ahead of the crack tip at higher applied stress levels. Otherwise the model appears to capture the essence of the crack growth behavior found for this composite reasonably well.

DISCUSSION

The main purpose of this paper has been to present results of an experimental micromechanics investigation of fatigue crack growth through a continuous fiber composite that exhibits fiber bridging, a continuation of earlier work on composites exhibiting no fiber bridging [1,2]. However, in addition to presenting the data, an effort has been made to show how fracture mechanics may be used to describe crack growth through the material.

Comparisons of published fatigue crack growth data for this composite [9,10,15] suggest that there is a great variability in properties from panel to panel. Thus, it is not known how typical are the results given for this panel of material with its specific processing history; however, for fatigue crack growth, fiber strength and strength distribution may be more important than details of consolidation. Interfacial debonding characteristics probably will be rather dependent on consolidation details because of the compressive residual stress developed across the interface due to thermal expansion mismatch. But what is important for fatigue crack growth is that the debonding stress only be

sufficiently low to prevent fiber fracture during crack passage. If the debonding stress is high, then fiber stresses will be increased in the crack wake, but the volume of fiber material sampled by this stress, which is proportional to the slip length, will be minimized. Conversely, a low debonding stress will result in lower stresses in bridging fibers, but more extensive slip distances, meaning that larger fiber volumes will be sampled. Fibers break because of flaws or irregularities in the fibers, and the probability of finding a fiber flaw is increased by increasing the volume of the fiber sampled by high stresses. Overall response of the material is highly dependent on the effects of stress and fiber volume (gage length) on fiber fracture.

A key finding of this work is that debond (slip) length is proportional to COD, thereby equalizing stress in the fibers, so that fiber stress is approximately independent of distance from the crack tip. This evidently occurs because of the "equilibrium" slippage between fiber and matrix that develops during the application of many thousands of loading cycles, and is the same reason for the relationship that develops between slip length and CODr due to residual stress relaxation.

One of the reasons fibers slip rather than break is that the coating can separate from the fiber and slippage can occur between layers in the coating. The existence of a carbon rich region in the coating is one of the reasons why slippage can occur within the coating layer. A good description of the layer characteristics of the fiber coating may be found in Ref. 21, which states that the coating "is made of a sequence of low shear strength pyrocarbon sublayers alternating with strong SiC+C sublayers." The reason that part of the coating remains on the fiber close to the crack plane is that when the fatigue crack breaks the matrix, the residual stresses clamping the fibers are relaxed so that sliding can occur between different layers of the coating rather than between the fiber and its coating, or the matrix and coating.

The large variation in magnitude of measured fiber stress and derived interfacial sliding stress is probably due to a number of factors. First, only a small part of the fiber surface is being sampled by the measurement technique. The process of matrix removal has not been uniform, relieving various amounts of residual stress. There were errors in measurement of fiber displacements which were magnified greatly in conversion to stress by the large fiber modulus, and then enlarged again by squaring the stress (in the case of analysis by

McCartney's model). There are also measurement errors and variation in COD. Fiber spacing is not uniform in the composite, causing a variation in residual stresses holding the fibers. Finally, the analysis from which interfacial shear stress is derived is for an isolated fiber, which is not very realistic, given the geometry shown in Fig. 1. Even with all these sources for variation, the measured and computed fiber stresses are in reasonably close agreement.

It must be concluded from the results presented that interfacial sliding stress is somewhere in the range of 150 to 300 MPa, with the most likely value being about 250 MPa. This value is in agreement with some of the measurements found in the literature [9,18], but differs greatly with others. Cox, et al. [23], derive values in the range of 5 to 15 MPa for other titanium alloy matrices, while McMeeking and Evans [8] find that values of 10 to 50 MPa must be used in their models if there is to be agreement with some of the published data. Yang, et al. [18], show, by the push-out method, that the specific matrix titanium alloy is important in determining the debond stress.

The question is, why are these great differences in debond stress found? The answer is unknown, but may be that all these measurements are not of the same quantity. In some cases, the stress to debond fiber from matrix has been measured directly; in other cases, the stress to cause sliding between matrix and fiber is determined by use of a model. Only fiber push-out or pull-out tests appear to give a direct measurement of this quantity, but even those tests are subject to interpretation. Further reading on this subject may be found in the work of Hsueh [24]. This issue remains unresolved.

These large differences in debonding stress may be linked to the experimental finding that fibers are debonding from the matrix ahead of the crack tip when applied stress is sufficiently large. For smaller stresses, debonding ahead of the crack tip was not found. When debonding occurs at or just ahead of the crack tip, stress in the matrix is increased; therefore, the crack tip stress intensity is increased. This factor is not included in any of the modeling efforts made to date, but the importance of this effect may not be great, although it has not been assessed yet in these terms. Debonding ahead of the crack tip may indicate that the conditions for fiber separation are more readily determined from strain incompatibility rather than from an analysis of stresses.

It is desirable to compare the experimental results with published fiber bridging models; however, an attempt to make these comparisons seems to indicate that none of these models is directly applicable. The models are presented without clear definitions of some of the parameters, and always in highly normalized parametric form, making direct comparison difficult because of uncertainties in knowing if assumptions used in the models match experimental conditions. Normalized parameters were computed using the experimental parameters for several of the models, with indications that the experimental results fell in regions where the models were not easily interpreted. Conversely, every effort has been made in this paper to give experimental data in a form where modelers can apply the results as they wish.

The model presented in **Appendices C and D** captures many of the essential elements of the experiments, but in its current form has only limited predictive capability. The next step would be to include some criteria for fiber fracture that would depend on a knowledge of the statistics of fiber strength as well as incorporating the effect of slip length, or volume, of the fibers exposed to high stress. Fiber strength statistics have been reported by Petitcorps, et al. [21], and these authors also addressed the dependence of fracture on volume (or length) of the fiber tested.

SUMMARY AND CONCLUSIONS

Fatigue cracks were grown perpendicular to the fibers through specimens having a center notched configuration, at stresses from 118 to 175 MPa. Crack growth rates from 10^{-10} to 10^{-7} m/cy were observed, and extensive fiber bridging and fiber fracture were observed. Extensive micromechanics measurements were made of parameters related to crack growth. The following conclusions were taken from the results and analysis:

1. Fatigue crack growth rate can either accelerate or decelerate with increasing crack length, depending on stress level.

2. Crack growth arrest with increasing crack length can occur at low stresses.

3. Relaxation of fiber and matrix residual stresses due to processing caused by crack passage results in a CODr from which slip length of fiber debonding can be determined.

4. Slip lengths up to 1 mm from the crack plane were measured after matrix removal.

5. Debonding between fiber and matrix occurs at several locations:
   - between fiber coating layers,
   - between fiber and coating,
   - between coating and matrix.

6. Fiber-matrix debonding stress can be determined from COD and other factors $\tau \approx 245$ MPa.

7. Fiber stress is in the range of 1.1 to 4.0 GPa and approximately independent of distance from the crack tip.

8. The Sneddon & Lowengrub equation for K_{tip} may be used to calculate fatigue crack growth rates, assuming:
   - stress is partitioned on the basis of area between cracked and uncracked parts of the specimen, and
   - pressure due to fiber bridging is independent of distance from the crack tip.

9. Crack growth rates are relatively insensitive to the exact number of bridging fibers.

10. Fibers break due to a combination of stress magnitude and length of slip (debonded) region.

ACKNOWLEDGEMENTS

This research was sponsored by the Office of Naval Research, Contract No. N00014-85-C-0206. The support and encouragement of Dr. Stephen Fishman, Contract Monitor, is much appreciated. Thanks to General Electric Aircraft Engines for permission to use some of the results obtained under their sponsorship. Thanks also to Dr. K.S. Chan for helpful discussions. The skill and assistance in specimen preparation and careful experimental work of John B. Campbell and the assistance with stereoimaging by James F. Spencer are also gratefully acknowledged.

REFERENCES

1. D.L. Davidson, K.S. Chan, A. McMinn and G.R. Leverant "Micromechanics and fatigue crack growth in an alumina fiber reinforced magnesium alloy composite" *Metall. Trans. A* **20A**, 1989, pp. 2369-2378.

2. K.S. Chan and D.L. Davidson "Effects of fiber interfacial strength on fatigue crack growth in a fiber reinforced Ti-alloy composite" *Metall. Trans. A* **21A**, 1990, pp. 1603-1612.

3. W.S. Johnson "Fatigue damage criteria: metal matrix and interfaces of continuous fiber reinforced metal matrix composites" in Mechanical and Physical Behavior of Metallic and Ceramic Composites, S.I. Anderson, H. Lilholt and O.B. Pederson, eds., Risø National Laboratory, Roskilde, Denmark, 1988, pp. 403-411.

4. V. Gerhold "Fatigue of continuous fiber-reinforced metal matrix composites" in Mechanical and Physical Behavior of Metallic and Ceramic Composites, S.I. Anderson, H. Lilholt and O.B. Pederson, eds., Risø National Laboratory, Roskilde, Denmark, 1988, pp. 35-50.

5. B. Budianski and J. W. Hutchinson and A.G. Evans "Matrix fracture in fiber reinforced ceramics" *J. Mech. Phys. Solids* **34**, 1986, pp. 167-189.

6. D.B. Marshall, B.N. Cox and A.G. Evans "The mechanics of matrix cracking in brittle-matrix fiber composites" *Acta metall.* **33**, 1985, pp. 2013-2021.

7. L.N. McCartney "Mechanics of matrix cracking in brittle-matrix fiber reinforced composites" *Proc. R. Soc. Lond. A* **409**, 1987, pp. 329-350.

8. R.M. McMeeking and A.G. Evans "Matrix fatigue cracking in fiber composites" *Mech. of Mater.* 9, 1990, pp. 217-227.

9. P.K. Wright, R. Nimmer, G. Smith, M. Sensmeier, and M. Brun "The influence of the interface on mechanical behavior of Ti-6Al-4V/SCS-6 composites" in Interfaces in Metal-Ceramic Composites, R.Y. Lin, R.J. Arsenault, G.P. Martins, and S.G. Fishman, eds., TMS, Warrendale, PA, 1990, pp. 559-581.

10. M.D. Sensmeier and P.K. Wright "The effect of fiber bridging on fatigue crack growth in titanium matrix composites" in Fundamental relationships between microstructures and mechanical properties of metal matrix composites, and M.N. Gungor and P.K. Liaw, eds., TMS, Warrendale, PA, 1990, pp. 441-457.

11. D.L. Davidson and A. Nagy "A low frequency cyclic loading stage for the SEM" *J. Phys. F* **11**, 1978, pp. 207-210.

12. D.L. Davidson "The observation and measurement of displacements and strain by stereoimaging" in Scanning Electron Microscopy/1979/II, SEM, Inc., AMF O'Hare, IL, 1979, pp. 79-86.

13. E.A. Franke, D.J. Wenzel, and D.L. Davidson "Measurement of micro-displacements by machine vision photogrammetry (DISMAP)" *Review of Sci. Instruments*, v. 62, 1991, pp. 1270-1279.

14. D.R. Williams, D.L. Davidson, and J. Lankford "Fatigue crack tip plastic strains by the stereoimaging technique" *Exper. Mech.* **20**, 1980, pp. 134-139.

15. K.R. Bain and M.L. Gambone "Fatigue crack growth of SCS-6/Ti-64 metal matrix composite" in Fundamental relationships between microstructures and mechanical properties of metal matrix composites, and M.N. Gungor and P.K. Liaw, eds., TMS, Warrendale, PA, 1990, pp. 459-470.

16. B.N. Cox, M.R. James, D.B. Marshall, and R.C. Addison "Determination of residual stresses in thin sheet titanium aluminide composites" *Metall. Trans. A* **21A**, 1990, pp. 2701-2707.

17. D.L. Davidson and J. Lankford "Fatigue crack growth for Ti-6Al-4V(RA) in vacuum and humid air" *Metall. Trans. A* **15A**, 1984, pp. 1931-1940.

18. C.J. Yang, S.M. Jeng and J.-M. Yang "Interfacial properties measurements for SiC fiber-reinforced titanium alloy composites" *Scripta metall. mater.* **24**, 1990, pp. 469-474.

19. Y. Le Peticorps, R. Pailler, and R. Naslain "The fiber/matrix interfacial shear strength in titanium alloy matrix composites reinforced by silicon carbide or boron CVD filaments" *Comp. Sci. and Technol.* **35**, 1989, pp. 207-214.

20. H. Tada, P. Paris, and G. Irwin "The Stress Analysis of Cracks Handbook, Del Research Corp., Hallertown, PA, 1973, p. 3.6

21. Y. Le Peticorps, M. Lahaye, R. Pailler, and R. Naslain "Modern boron and SiC CVD filaments: a comparative study" *Comp. Sci. and Technol.* **32**, 1988, pp. 31-55.

22. Textron Specialty Materials Pamphlet, anon, undated, obtained 1989.

23. B.N. Cox, M.S. Dadkhah, M.R. James, D.B. Marshall, W.L. Morris, and M. Shaw "On determining temperature dependent interfacial shear properties and bulk residual stresses in fibrous composites" *Acta metall. mater.* **38**, 1990. pp. 2425-2433.

24. C-H. Hsueh "Theoretical comparison of two loading methods in fiber pull-out tests" *Mater. Sci. and Eng.* **A130**, 1990, pp. L11-L15.

25. T.G.F. Gray "Convenient closed form stress intensity factors for common crack configurations" *Int. J. Fracture* **13**, 1977, pp. 65-75.

Appendix A - Estimation of slip distance from CODr

The repeated slip between fiber and matrix over thousands of cycles that is caused by passage of the crack allows the fiber and matrix to relieve residual stresses caused by cooling from elevated (processing) temperatures. The equilibrium thus attained results in a residual crack opening displacement, CODr. The following analysis relates CODr and slip distance between fiber and matrix, l_s. CODr results from elongation of the fibers, l_f, and contraction of the matrix, l_m, calculated as follows:

$$CODr = l_f + l_m$$

$$l_f = l_s(\sigma_{rf}/E_f)$$

$$l_m = l_s(\sigma_{rm}/E_m)$$

Definitions of these quantities are made with assistance of Fig. A1. Residual stresses in the fiber and matrix due to cooling through the temperature range ΔT ($\approx$ 900°C) are σ_{rf} and σ_{rm} , respectively, and are calculated from the difference in thermal expansion coefficients $\Delta\alpha$ using

$$\sigma_{rm} = \Delta\alpha\Delta T/S_c$$

$$\sigma_{rf} = -\sigma_{rm}(1-f)/f$$

where f = vol. or area fraction of fiber in the composite, and the composite compliance $S_c = [(1-f)/fE_f+1/E_m]$.

$$CODr = 2l_s\varepsilon_{rc}$$

where $\varepsilon_{rc} = (\sigma_{rf}/E_f + \sigma_{rm}/E_m)$ is the composite residual strain.

Using the values shown in Table 1 in this analysis gives

σ_m = 360 MPa σ_{rf} = - 500 MPa ε_{rc} = 0.002

which then gives the estimate of l in terms of CODr as

$$l_s = CODr/2\varepsilon_{rc} = 250\ CODr$$

Appendix B - Estimation of interfacial shear stress from COD and CODr

An estimate of the shear stress between matrix and fiber may be derived from the Crack Opening Displacement (COD) caused by applied stress (σ_a). The relationships shown in Fig. 1B will assist in understanding the following derivation.

COD at maximum load is composed of the elongation in the unbroken fiber bridging the crack, CODr, and elongation of the matrix caused by the shear stress τ acting on the fiber.

$$COD/2 = \varepsilon_f l_s + CODr/2 - l_s\tau/G_m$$

where G_m = shear modulus of the matrix. From Appendix A, $CODr/2 = l_s\varepsilon_{rc}$. Combining and rearranging gives

$$\tau/G_m = \varepsilon_f + \varepsilon_{rc} - COD/2l_s$$

The ratio $COD/2l_s$ is approximately constant (ave. = .0043) for the measurements that were made, as shown in Table 5. Using these data along with fiber stresses given in Table 4, shear stresses ranging from 15 to 580 MPa were computed for specimen 4, with an average τ = 245 MPa with a standard deviation of 197 MPa.

Appendix C - Estimation of fiber stress from applied stress

Fiber stress may be estimated by partitioning the applied load according to cracked and uncracked areas. Fibers within the bridged area support all the load on the cracked area, while in the uncracked area, both fibers and matrix support the load. Estimates of fiber stress were made by computing the load supported by the uncracked area, subtracting that load from total applied load and dividing by the area of the unbroken fibers bridging the cracked area. The area of the notch was assumed to bear no load, as were regions of the fatigue crack where fibers were broken. The load that these regions would have born was shifted to the bridged crack and uncracked region. The result of this calculation is the average fiber stress, given in italics in Table 4.

Appendix D - Integration of the McCartney modified Sneddon & Lowengrub equation for crack tip stress intensity

The basic equation for crack tip stress intensity factor that accounts for fiber bridging is

$$K_{tip} = \{\sqrt{(4a/\pi)}\}\int\{(\sigma_a - p(x)) / \sqrt{(a^2 - x^2)}\}\, dx \qquad (D1)$$

It has been necessary to integrate this equation to include two regions: (1) a non-bridged region comprised of the notch and crack with broken fibers, and (2) fiber bridged region. Integration is easier than performed by other investigators because the term p(x) is constant, for reasons given in the text. The geometry of the problem being solved is shown in Fig. D1. For present purposes, the coordinate system origin is changed from specimen centerline to crack tip. This is accomplished by setting x = c - d and substituting y = d/c, which changes eq. (D1) to

$$K_{tip} = \{\sqrt{(4a/\pi)}\}\sigma_a\int dy / \sqrt{(2y - y^2)} - \{\sqrt{(4a/\pi)}\}p_o\int dy / \sqrt{(2y - y^2)} \qquad (D2)$$

The integrals are between 1 and 0; however, p = 0 over the range 1 to b, where b = length of bridging zone/crack length, σ_a = applied stress, and p_o = the pressure along the crack flank caused by bridging fibers. The first integrand is the K due to applied stress and the second that due to fiber bridging. Integrating and inserting the limits gives

$$K_{tip} = \{\sqrt{(4aF/\pi)}\}\{\sigma_a\pi/2 + p_o(\cos^{-1}(b) - \pi/2)\} \qquad (D3)$$

where the geometric factor F has been added for a center notched specimen configuration; F is calculated from the formulation by Gray [25].

Experimental results were compared to eq. (D3) by inserting the controlling experimental parameters: σ_a and a, then estimating and inserting p_o and computing K_{tip}, which was used to compute the crack growth rate. Fiber stress was computed from the estimate of p_o. The results of this calculation were evaluated by comparison with the measured crack growth rate and fiber stress.

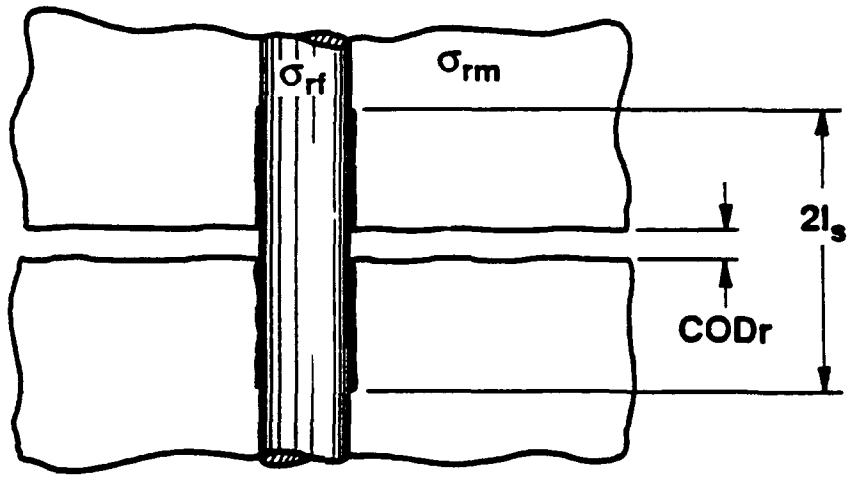

Fig. A1 Relationship between CODr, slip distance, and residual stresses.

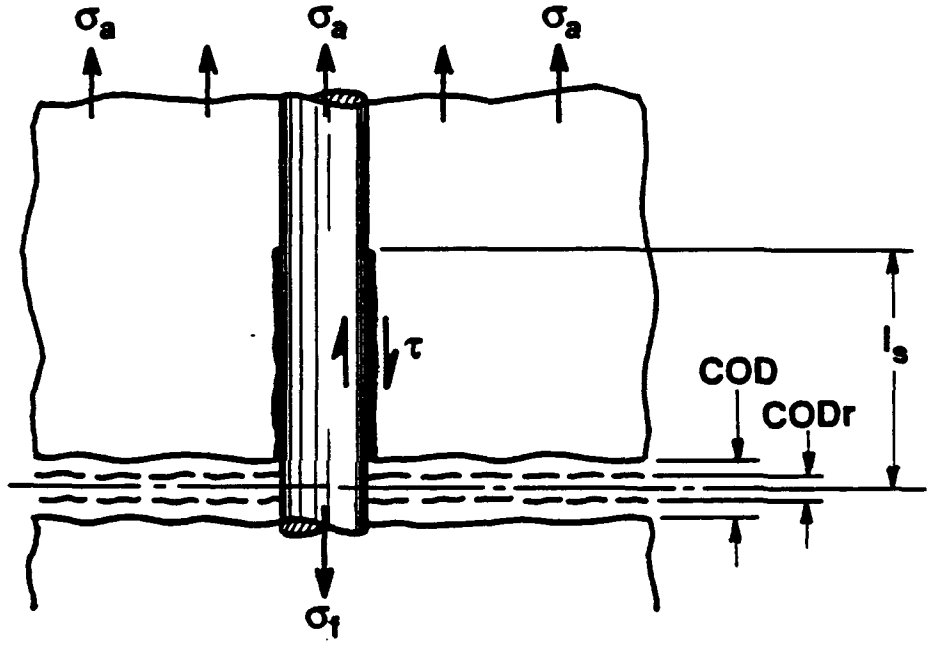

Fig. B1 Stresses on loaded crack and their relation to COD.

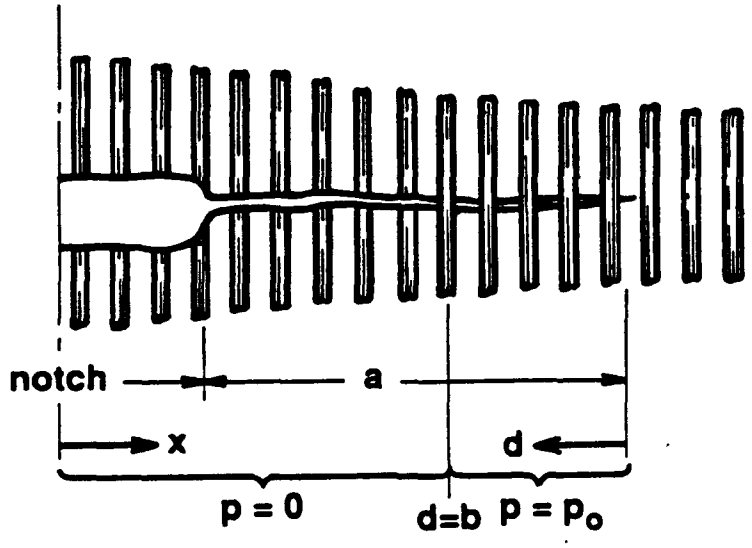

Fig. D1 Partially bridged crack showing axes and dimensions.

Table 1
Parameters characterizing the Composite

Tensile modulus of fiber	E_f	400 GPa
Tensile modulus of matrix	E_m	110 GPa
Shear modulus of matrix	G_m	73 GPa
Tensile modulus of composite	E_c	230 MPa
Poisson's ratio for fiber	υ	0.25
Volume fraction of fibers	f	0.42
Volume fraction of matrix	m	0.58
CTE of fiber	a_f	$5x10^{-6}/°C$
CTE of matrix	a_m	$10x10^{-6}/°C$

Table 2
Center Notched Specimens
Test Parameters

Spec. No.	No. cycles kHz	Stress Range MPa	Crack 1 crack length mm		Crack 2 crack length mm	
			start	end	start	end
1	0-210	150	4.10	4.56	4.10	4.38
	210-440	162	4.56	4.75	4.38	4.58
	440-907	176	4.75	5.78	4.58	5.35
2	0-145	180	5.06	6.67	5.06	6.75
3	0-125	154	3.05	3.48	3.05	3.35
4	0-190	118	4.02	5.08	4.02	5.22
	190-561	145	5.08	5.10	5.22	5.27
	561-1016	175	5.10	6.59	5.27	5.97

Table 3
Fiber Damage and Crack Opening
Specimen 4, 1016 kcy

Fiber No.	Meas. slip distance mm	CODr μm	Calc. slip distance mm	COD μm	COD/2l_s 10^{-3}
Crack 1					
1	1.0	2.5	0.63	6.3	6.3
2	0.86	2.0	0.55	6.8	7.1
3	0.64	4.0	1.0	5.7	8.9
4	0.72	5.0	1.25	5.4	7.6
5	0.54	4.0	1.0	5.1	9.5
6	0.84	3.0	0.75	4.9	6.0
7	0.52	2.0	0.55	4.5	8.7
8	0.21	0.8	0.20	4.1	19.3
9	0.43	0.6	0.15	3.5	8.23
10	0	0.5	0.125	3.0	--
11	0	0.3	0.075	2.5	--
12	0	0	--	1.7	--
Crack 2					
1	0.92	-	-	7.7	8.4
2	0.82	-	-	7.2	8.8
3	0.80	3.2	0.80	6.7	8.4
4	0.79	3.5	0.87	6.1	7.8
5	0.65	3.7	0.92	5.6	8.6
6	0.56	2.4	0.60	5.0	8.8
7	0.60	1.7	0.42	4.2	7.1
8	0.45	0.8	0.20	3.5	7.8
9	0	-	-	1.0	2.3

Table 4
Mode I Crack Opening Displacment Measurements
COD I = $C_o\sqrt{d}$

Specimen No.	Stress MPa	Cycles (kcy)	Crack No.	C_o (μm)
3	154	125	1	0.225
4	118	190	1	0.039
			2	0.033
	145	561	1	0.038
			2	0.022
	175	1016	1	0.13
			2	0.185

Table 5
Measured Fiber Stresses, Interface Condition
and Interface Debonding stresses
(McCartney's Model)

No. cycles (kilocycles)	Crack No.	Fiber No.	Axial Stress (GPa)	Interface Condition (DB=debond)	Calculated Shear Stress (GPa)
Specimen 3					
126	1	1	3.3	DB	48
		2	4.0	DB	102
		3	3.9	DB	ck tip
Calculated fiber stress (GPa)			*3.5*		
Specimen 4					
190	2	3	1.2	B	24
		4	3.4	B	200
		5	4.1	B	350
		6	1.8	B	138
		7	1.1	B	--
Calculated fiber stress (GPa)			*1.9*		
561	1	1	XX	DB	
		2	XX	DB	
		3	3.5	DB	190
		4	1.9	DB	91
		5	2.8	B	163
		7	1.0	B	--
		8	2.8	B	--
Calculated fiber stress (GPa)			*2.5*		
561	2	3	XX	DB	
		4	2.4	DB	174
		5	1.4	B	100
Calculated fiber stress (GPa)			*2.1*		
1016	1	1-10	XX	DB	
		12	3.2	DB	--
		13	2.4	DB	--
		14	2.7	DB	--
		15	2.0	DB	--
		16	4.1	B	--
1016	2	1-7	XX	DB	
		8	2.7	DB	100
		9	3.5	DB	--
		12	2.0	DB	--
		13	1.3	DB	--
Calculated fiber stress (GPa)			*3.5*		

Notes: XX denotes broken fibers -- denotes fibers ahead of crack tip

Table 6
Model Results
Specimen 4

Cycle (kcy)	Applied stress (MPa)	Crack length (mm)	Press. p_o (MPa)	Fiber stress (GPa)	Bridg. rows max	Bridg. rows model	K_a (MPa$\sqrt{m}$)	K_{tip} (MPa$\sqrt{m}$)	Growth rate calc. (10^{-10} m/cy)	Growth rate meas. (10^{-10} m/cy)
190	118	1.06	668	1.9	5	5	18.7	5.4	74	80
		1.20	686	2.0	5	5	19.1	5.5	79	100
561	145	1.18	924	2.3	5	5	23.5	5.1	62	3
		1.25	780	2.1	6	6	23.7	5.1	62	1
791	175	1.35	1280	3.1	6	4.5	29.1	6.3	120	10
		1.48	1245	3.0	7	4.7	29.5	6.4	128	8
831	175	1.84	1395	3.4	9	4.2	31.4	6.8	157	100
		1.60	1280	3.4	7	4.7	30.2	6.6	138	40
871	175	2.32	1700	3.4	11	4	33.8	7.4	200	90
			*1805	*4.6				*5.8	*90	90
		1.82	1560	4.8	9	4	31.3	6.9	157	50
			*1700	*4.0				*4.7	*50	50
1016	175	2.57	1410	3.4	12	5	35.2	7.7	224	10
		1.95	1280	3.1	9	5	31.9	7.0	164	10

* denotes computation using the pressure shown.

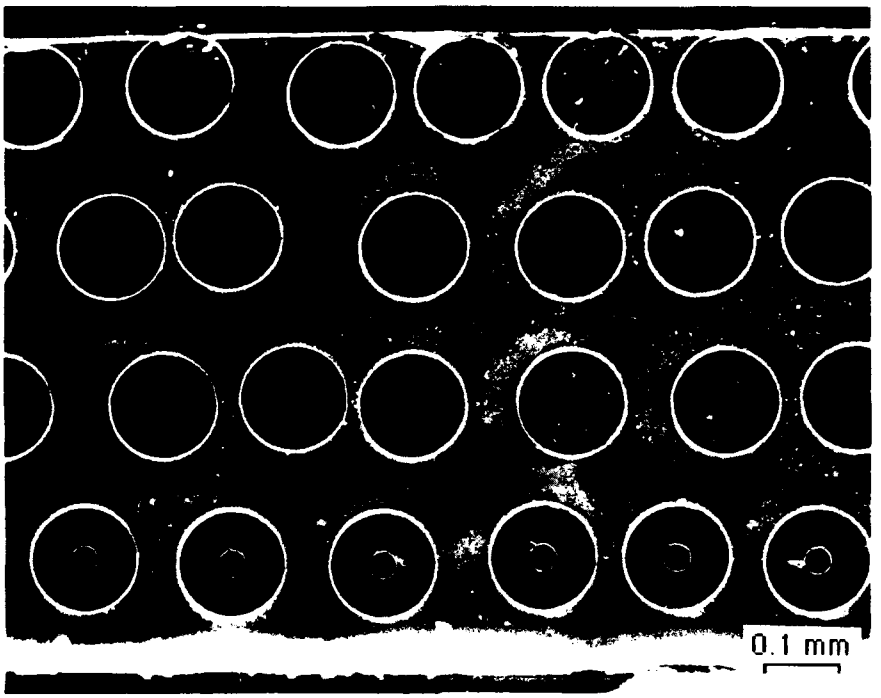

Fig. 1 Cross section through the thickness of the composite showing the four layers of fibers covered at the outer surface by a thin layer or matrix. The material is well consolidated between fibers, and fiber spacing is somewhat irregular.

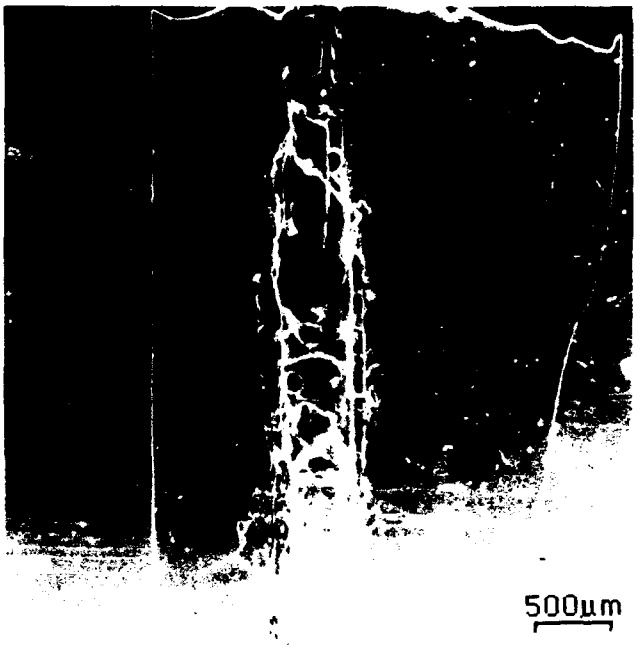

(a)

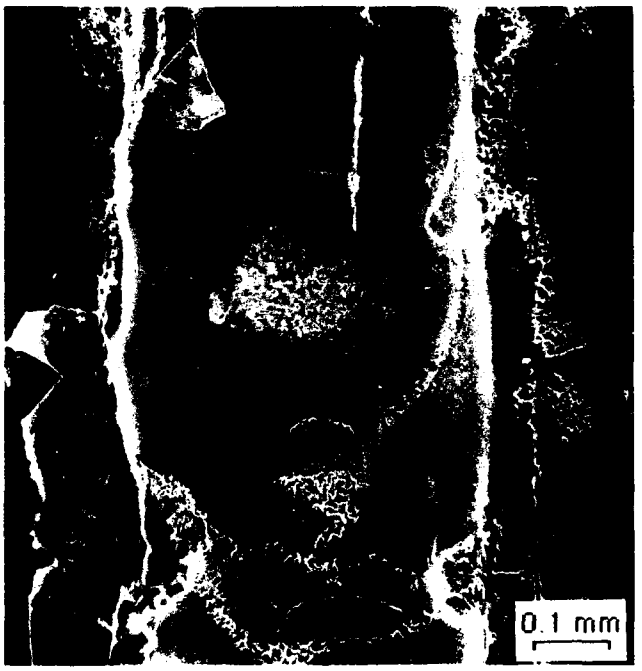

(b)

Fig. 2 (a) Appearance of composite at one end of the center notch after removal of material to create ports into the fibers. (b) Higher magnification view of several fiber ports near end of fatigue crack.

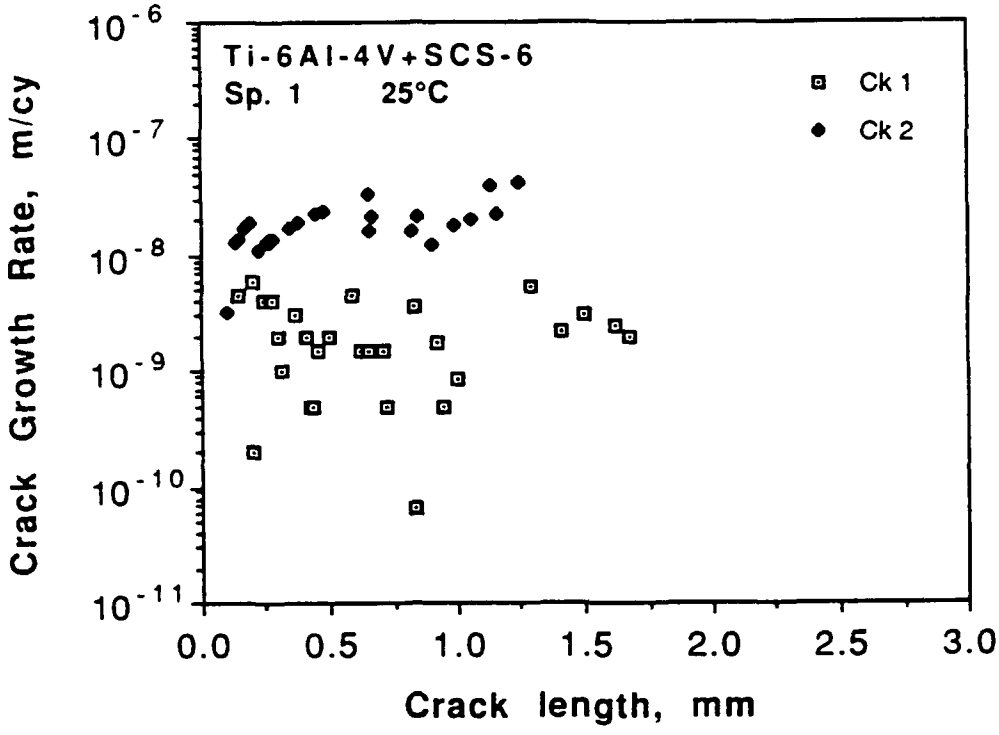

Fig. 4 Crack growth rates in center notched specimen 1. Crack growth data only from side A of the specimen, cracks 1 and 2.

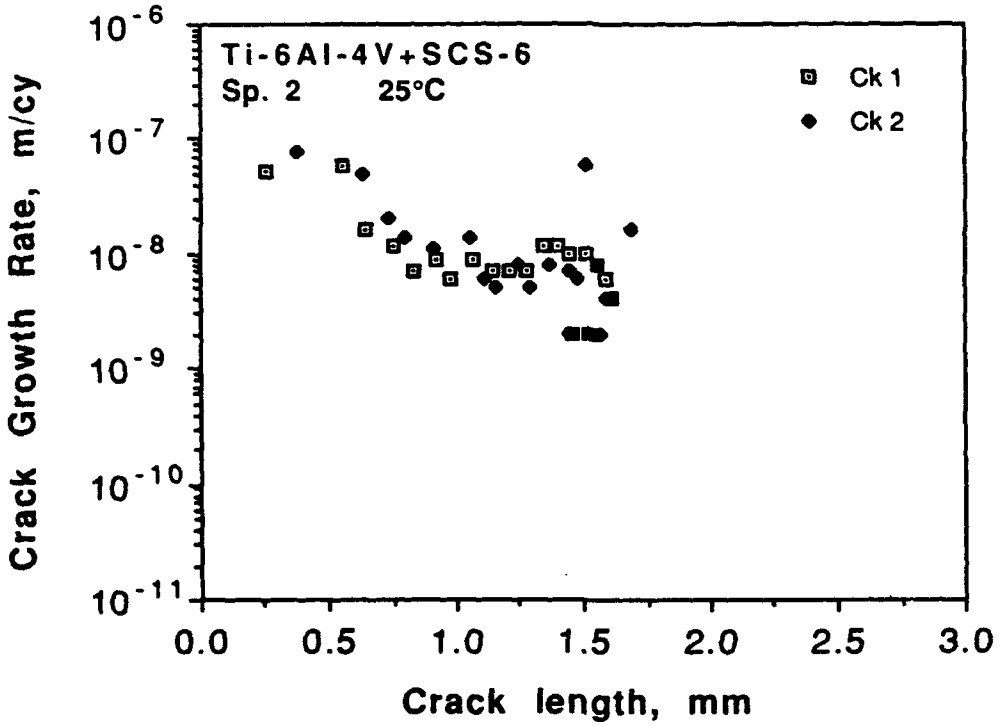

Fig. 5 Crack growth rates in specimen 2.

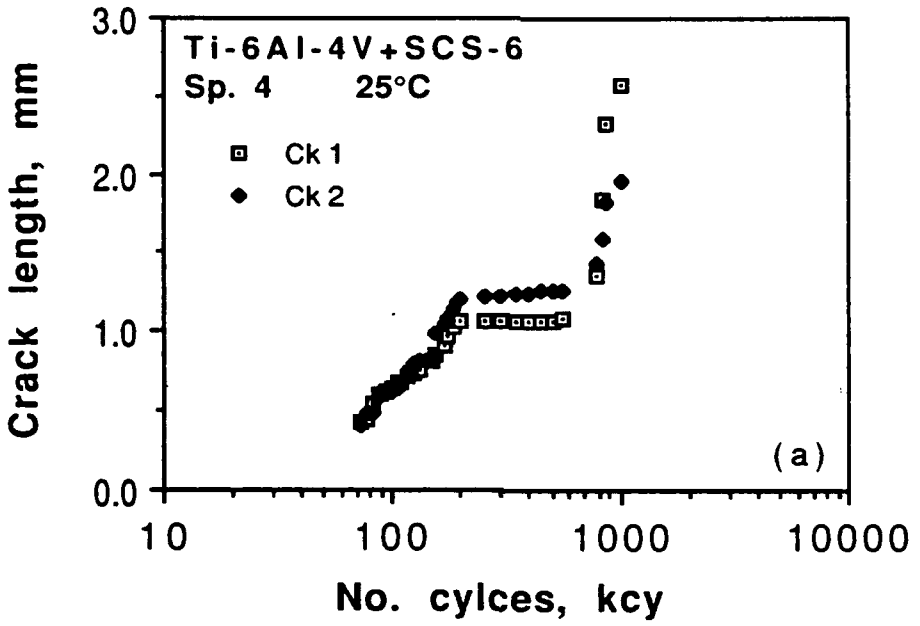

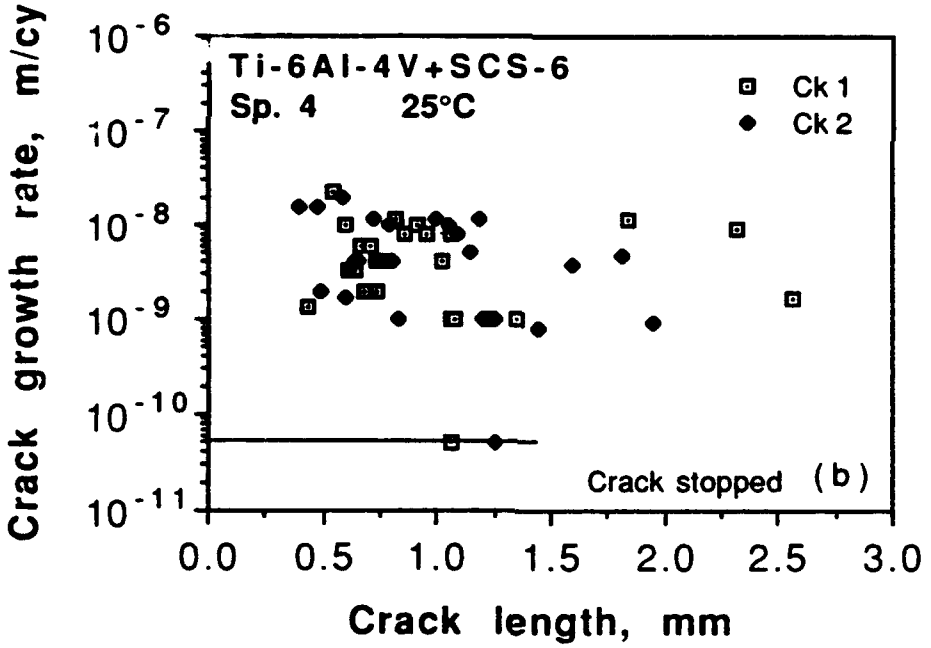

Fig. 6 (a) Specimen 4, crack length vs cycles showing the effect of stress level. (b) Fatigue crack growth rates corresponding to the data in (a).

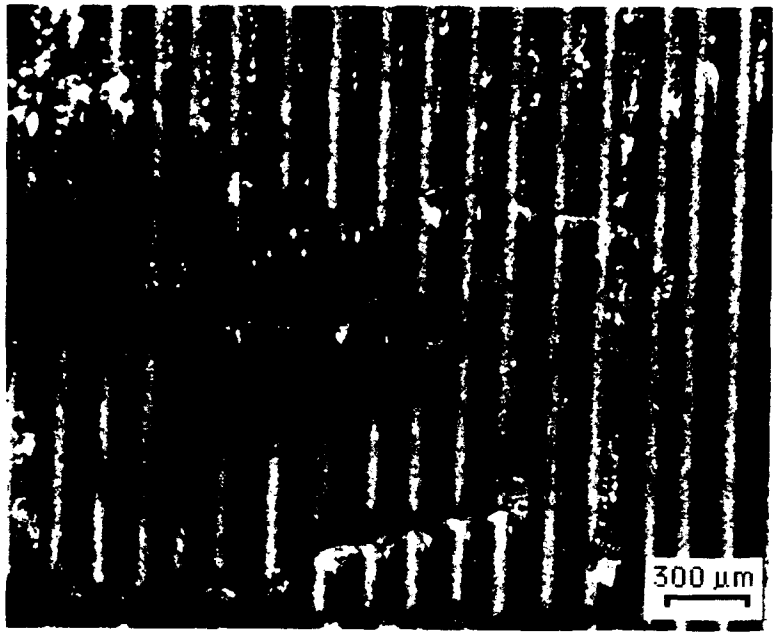

(a)

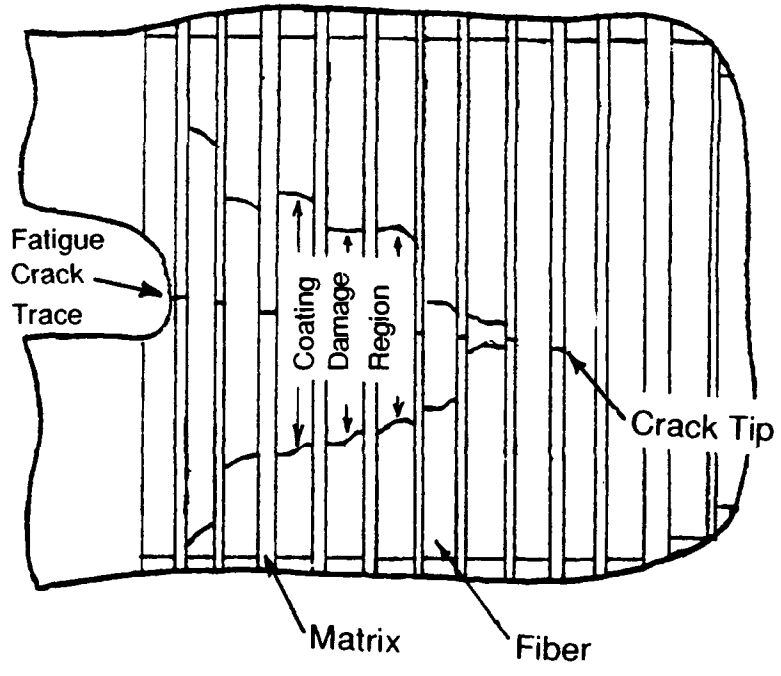

(b)

Fig. 7 Optical micrograph of (a) fiber damage beneath the crack in specimen 1. Matrix removal in two steps, by electropolishing, created the ridge seen near the crack line. (b) A sketch of the extent of fiber damage behind the crack tip. The outer coating of the bridging fibers is cracked for a considerable distance away from the crack plane, but not ahead of the crack tip.

Fig. 8 Higher magnification view of fiber damage in specimen 1 showing the nature of the coating cracking. Along the crack plane, the outer coating appears cracked and sometimes removed, but not the inner coating.

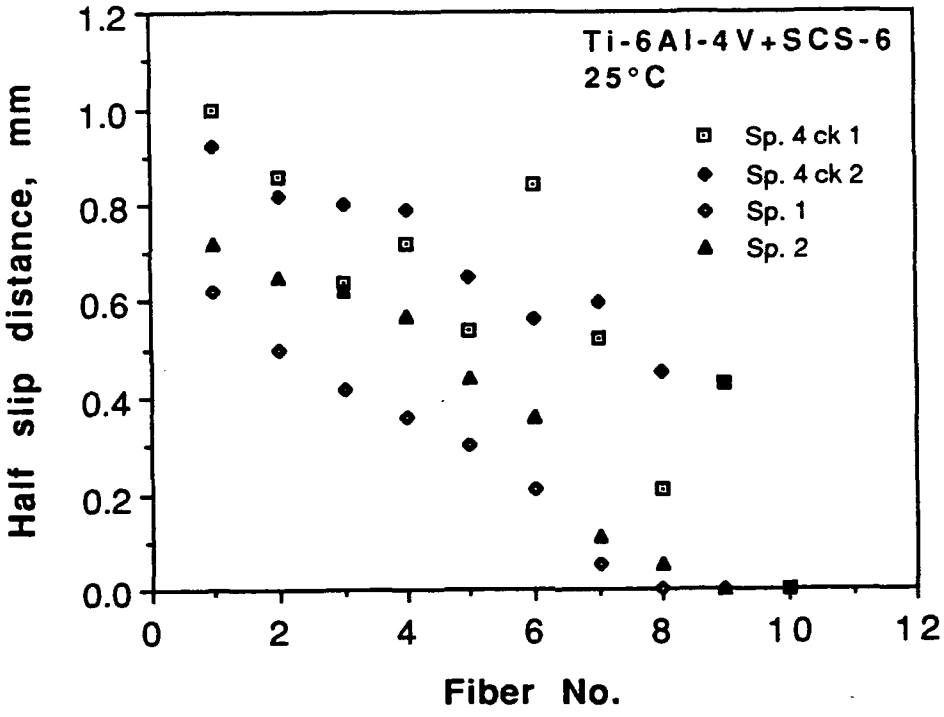

Fig. 9 Slip distance, as determined by fiber damage, as a function of distance along the crack plane, for specimens 1, 2 and 4.

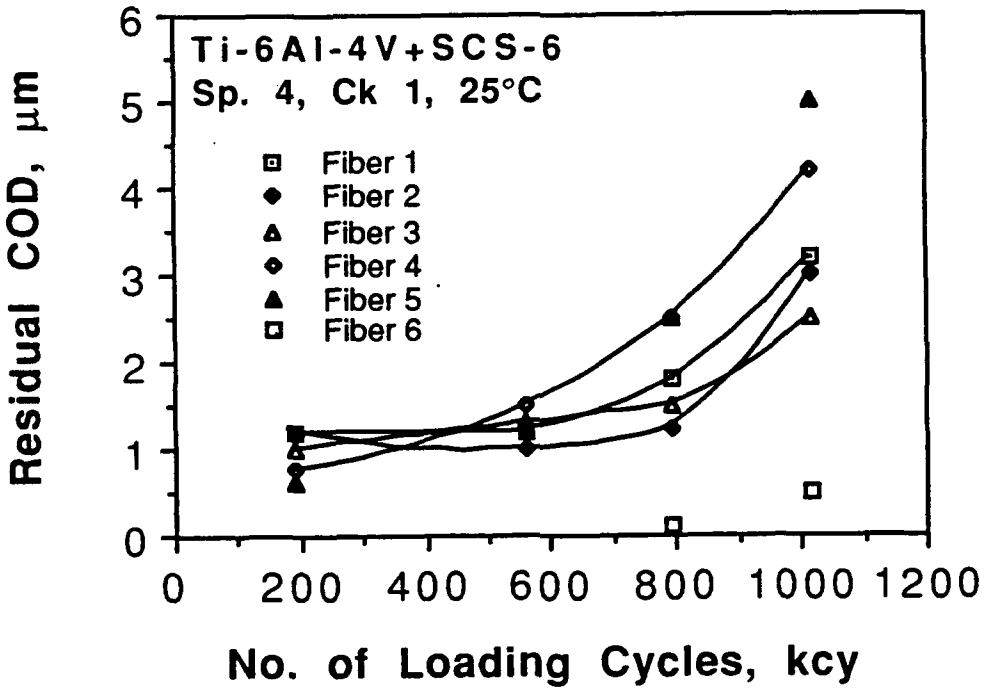

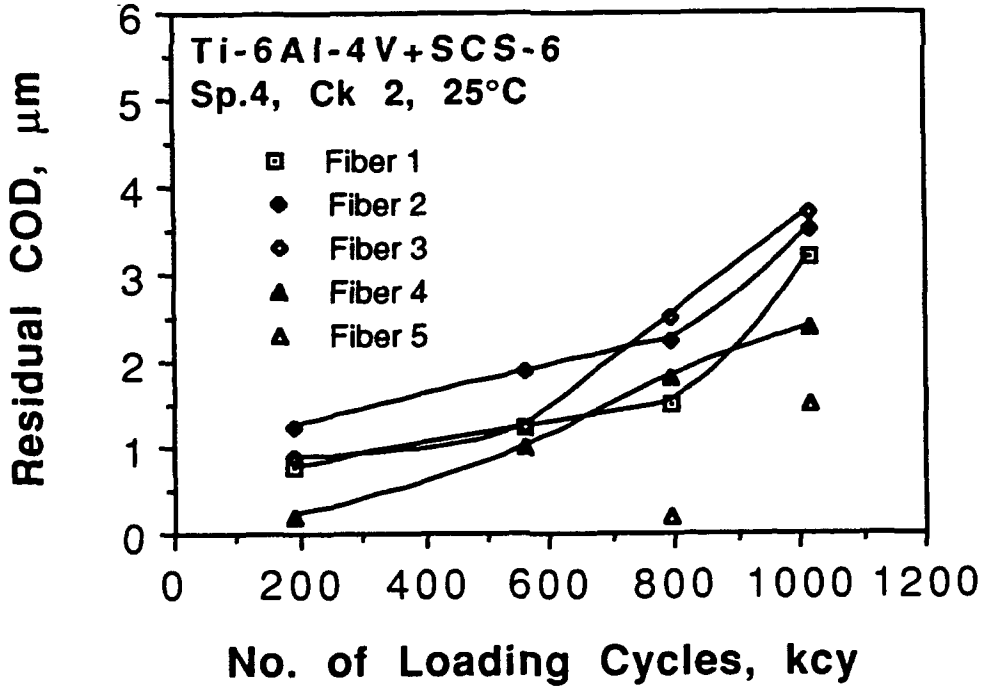

Fig. 10 Residual Crack Opening Displacment (CODr) as a function of the number of loading cycles for specimen 4, (a) crack 1, and (b) crack 2.

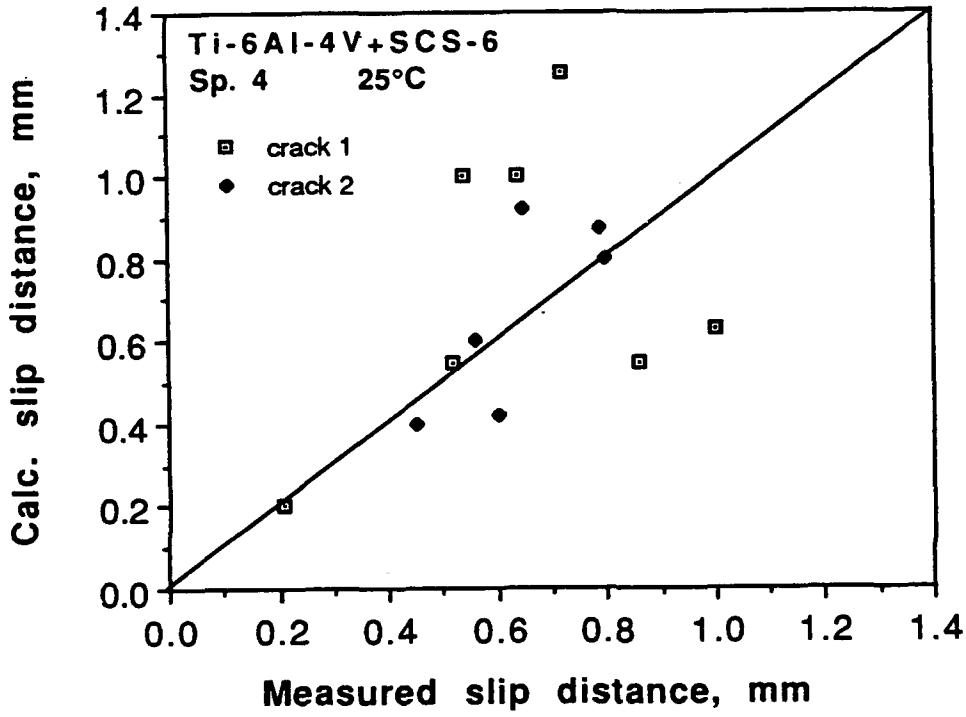

Fig. 11 Comparison of slip distances calculated from CODr and measured.

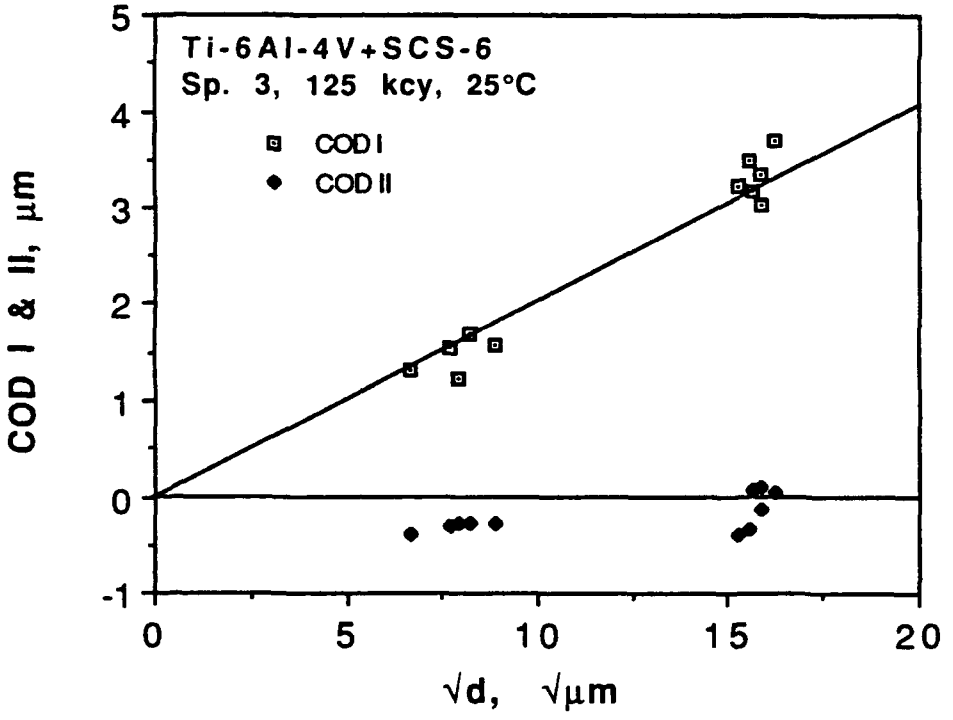

Fig. 12 Specimen 3, COD as a function of the distance from the crack tip.

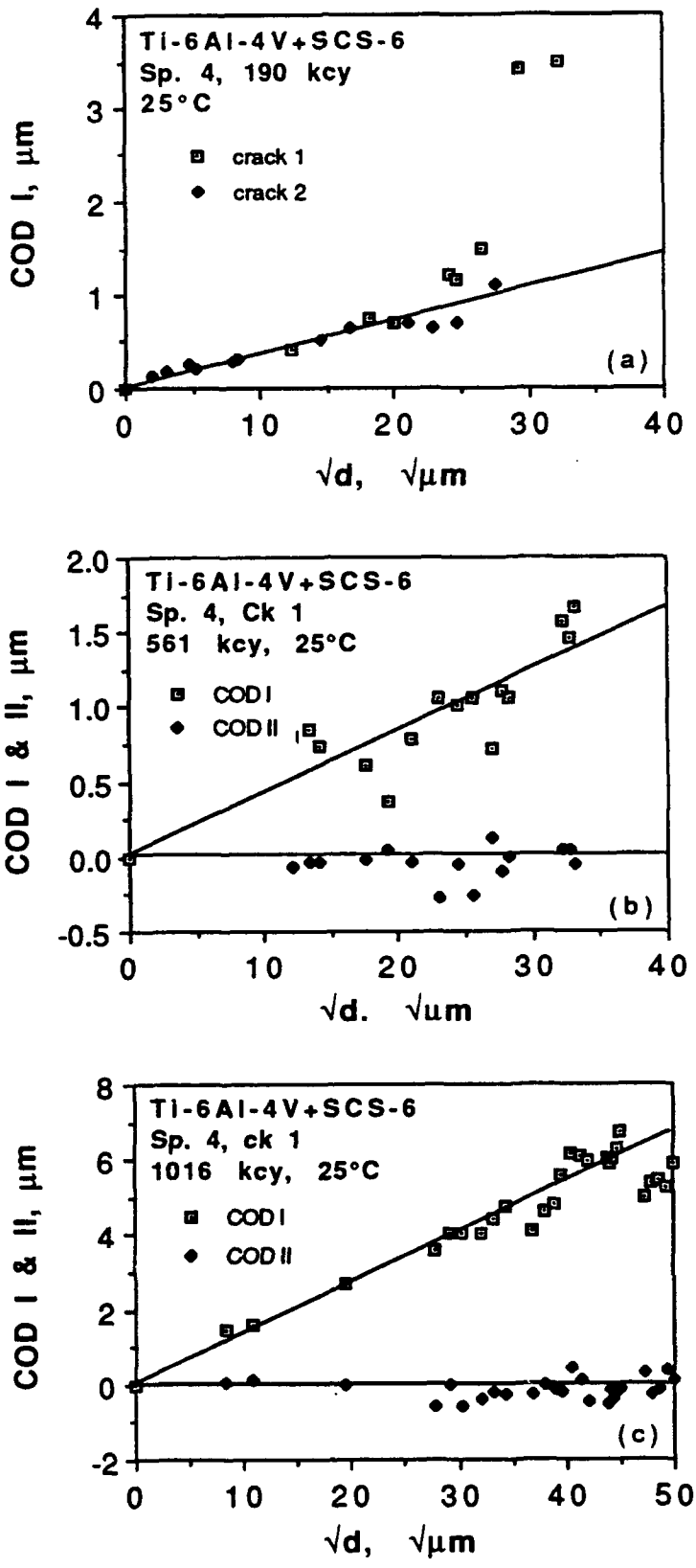

Fig. 13 Specimen 4, COD as a function of the distance from the crack tip for several crack lengths. (a) 190 kcy, (b) 561 kcy, and (c) 1016 kcy.